Columnar Structures from Asymmetrically Tapered Biphenylamide

Soo-Jin Park,[†,‡,%] Seok-Ho Hwang,[†,§] Namil Kim,[#] Shiao-Wei Kuo,[$] Hak Yong Kim,[%] Seul-Ki Park,[‡] Young-Jin Kim,[‡] Changwoon Nah,[‡] Joong Hee Lee,[‡] and Kwang-Un Jeong*[,‡]

Polymer Materials Fusion Research Center and Department of Polymer-Nano Science and Technology, Chonbuk National University, Jeonju 561-756, Korea, Department of Polymer Science and Engineering, Dankook University, Yongin 448-701, Korea, Department of Polymer Engineering, The University of Akron, Akron, Ohio 44325-0301, Department of Materials Science and Optoelectronic Engineering, National Sun Yat-Sen University, Kaohsiung 804, Taiwan, and Department of Textile Engineering, Chonbuk National University, Jeonju 561-756, Korea

Received: June 17, 2009; Revised Manuscript Received: August 18, 2009

An asymmetrically tapered *N,N′-tris*[[(2-dodecylaminocarbonyl)ethyl]methyl]-4-biphenylamide (asym-C_{12}PhA, where n is the number of carbon atoms in the alkyl chains, $n = 12$) was newly designed and synthesized. In this asymmetrically tapered asym-C_{12}PhA biphenylamide, *H*-bondable hydrophilic amide moieties are located at between a rigid hydrophobic biphenyl rod and three flexible hydrophobic alkyl chains. Computer energy minimization indicated that three-dimensional (3D) geometry of asym-C_{12}PhA biphenylamide looks like a cone with dimensions of 3.01 nm in height and 1.44 nm in bottom radius. Phase transitions and supramolecular structures were identified utilizing the combined techniques of differential scanning calorimetry, 1D wide-angle X-ray diffraction (1D WAXD), Fourier-transform infrared spectroscopy, and solid-state ^{13}C nuclear magnetic resonance analyses. The asym-C_{12}PhA self-assembled into a highly ordered columnar mesophase just below the isotropization temperature and then transformed to 3D columnar crystalline phase (Φ_{Cr}) on further cooling. Selected area electron diffractions in transmission electron microscopy (TEM) along with 1D WAXD and cross-polarized optical microscopy suggested that discotic building blocks were constructed by rotating 120° of three asym-C_{12}PhA with respect to neighboring ones and the tmb (top-middle-bottom) stacked discotic building blocks further self-organized into columns. These columns are laterally intercalated to form the Φ_{Cr} phase. On the basis of the TEM image and polyethylene surface decoration technology, it was identified that the self-assembled asym-C_{12}PhA fibers with ~1 μm in diameter and several millimeters in length were braids of tiny single crystals.

Introduction

Even though the recent rapid development in liquid crystal display (LCD) technology has mainly been achieved on the basis of calamitic (rod-like) LCs, the structures and dynamics of discotic columnar molecules have been extensively studied in academia and industry because of their extraordinary properties, such as one-dimensional (1D) electrical conductivity, fast photoconductivity, and ferroelectricity.[1−15] In general, discotic columnar phases were induced by the $\pi-\pi$ interactions between the disk-like aromatic supermolecules which are the individual giant molecules made of disk-like aromatic rigid cores with covalently bonded flexible alkyl tails.[2,3] Recently, a process of self-assembly through noncovalent interactions including hydrogen-bonding, electrostatic, $\pi-\pi$ stacking, van der Waals interactions, and hydrophobic−hydrophilic effects paves a new road for the design and synthesis of functional organic materials.[16−41] One of the examples is hydrophobic−hydrophilic effects in block copolymers. Incompatible yet chemically bonded components in block copolymers induces the nanophase separation to form cubic, lamellar, hexagonal columnar, or bicontinuous gyroid structures.[16] *H*-bonding in supra-molecular structures also becomes a major tool to program building blocks because of its moderate bonding energy, directionality, selectivity, and reversibility.[23−41] In *H*-bonding systems, self-assembled columnar structures are not formed by the self-organization of discotic supermolecules but rather constructed by the self-assembly of supra-molecular discs as building blocks generated via intra/intermolecular *H*-bonding.[23−41] By the combination of different driving forces in self-assembly, various structures such as smectic, laminated, and polygonal columnar phases can be induced in different length scales depending on the volume fractions of each component and interactions.[23−41]

From the recent study regarding self-assembly of symmetrically tapered bisamides, a self-assembled discotic building block can be generated through intermolecular *H*-bonding and nanophase separation of the rigid cores and alkyl tails.[42−46] These supra-molecular discs were further self-organized into oblique columnar phases. However, there remains an unsolved question: Is a columnar structure constructed even from an asymmetrically tapered biphenylamide rod-like molecule? If the answer is yes, what is the molecular self-assembled structure from asymmetrically tapered biphenylamide molecules?

An asymmetrically tapered *N,N′-tris*[[(2-dodecylaminocarbonyl)ethyl]methyl]-4-biphenylamide (asym-C_{12}PhA, $n = 12$) was newly synthesized in order to understand the molecular self-assembly of asymmetric biphenylamide molecule containing

* Corresponding author. E-mail: kujeong@chonbuk.ac.kr.
† These authors contributed equally to this work.
‡ Polymer Materials Fusion Research Center and Department of Polymer-Nano Science and Technology, Chonbuk National University.
§ Dankook University.
# The University of Akron.
$ National Sun Yat-Sen University.
% Department of Textile Engineering, Chonbuk National University.

10.1021/jp905672s CCC: $40.75
Published on Web 09/18/2009

the *H*-bondable amine functions between an aromatic core and flexible alkyl tails. It mainly consists of three different parts: *H*-bondable hydrophilic amide moieties, a rigid hydrophobic biphenyl aromatic core, and three flexible hydrophobic alkyl chains at one end of biphenyl aromatic rod. One-dimensional wide-angle X-ray diffraction (WAXD) and differential scanning calorimetry (DSC) techniques were used for thermal and structural transition analyses. The *H*-bonding between amine (N−H) and carbonyl (C═O) groups and the dynamic conformational changes of the aromatic and aliphatic parts of asym-C_{12}PhA biphenylamide at different temperatures were monitored using Fourier-transform infrared spectroscopy (FT IR) and solid-state carbon-13 nuclear magnetic resonance (^{13}C NMR). In addition to 1D WAXD, the phase structures were further identified by selected area electron diffractions (SAED) in transmission electron microscopy (TEM) from single crystals. The phase morphologies in the ordered phases were further investigated via cross-polarized optical microscopy (POM).

Experimental Section

Materials and sample preparation. A asymmetrically tapered *N,N′-tris*[[(2-dodecylaminocarbonyl)ethyl]methyl]-4-biphenylamide (asym-C_nPhA, where *n* is the number of carbon atoms in the alkyl chains, $n = 12$) was newly designed and synthesized via simple peptide coupling reactions.[47−50] The detailed synthetic procedures were shown in Scheme 1. The final compound was purified through repeated chromatography with a silica gel using an acetone−benzene (5:95) mixture as an eluting solvent, followed by recrystallization from an ethanol−benzene mixture. The purity was verified by thin layer chromatography (TLC) and proton nuclear magnetic resonance (^{1}H NMR). Chemical structure of asym-C_{12}PhA was confirmed by ^{1}H NMR spectroscopy in $CDCl_3$ solution: δ 8.01 (s, −CON*H*−, 4H), 7.94 (d, 2,6-Ar*H*, 2H), 7.66 (d, 3,5-Ar*H*, 2H), 7.61 (d, 2,6-Ar′*H*, 2H), 7.45 (dd, 3,5-Ar′*H*, 2H), 7.37 (dd, 4-Ar′*H*, 1H), 3.20 (m, −CONHC*H*$_2$−, 6H), 2.17 (m, −C(CH$_2$C*H*$_2$−)$_3$, 6H), 1.87 (m, −C(C*H*$_2$CH$_2$−)$_3$, 6H), 1.23 (m, −CONHCH$_2$(C*H*$_2$)$_{10}$CH$_3$, 20H), 0.89 (m, −CONHCH$_2$(CH$_2$)$_{10}$-C*H*$_3$, 9H).

For one-dimensional (1D) wide-angle X-ray diffraction (WAXD) measurements, films with a thickness of about 1 mm were prepared by melting the compounds on an aluminum plate. The samples prepared for POM analysis had a typical thickness of 10 μm and they were melt-processed between two bare cover glass sides. The samples for Fourier transform infrared spectroscopy (FT IR) were prepared by film casting from a $CHCl_3$ dilute solution onto KBr plates. The powder samples were used for solid-state carbon-13 (^{13}C) nuclear magnetic resonance (NMR). Thin film samples prepared for transmission electron microscopy (TEM) via solution casting from a 0.05% (w/v) chloroform solution onto carbon-coated mica had a thickness of 50−150 nm. After crystallization and annealing processes, the films were floated onto the water surface and recovered using the TEM copper grids.

Equipment and Experiments. The thermal behavior of the phase transitions was studied using a Perkin-Elmer PYRIS Diamond DSC equipped with an Intracooler 2P apparatus. The temperatures and heat flows were calibrated using standard materials at various cooling and heating rates ranging from 2.5 to 40 °C/min. In order to eliminate previous thermal histories, the heating process always preceded the cooling experiments. The transition temperatures were determined by measuring the onset, peak, or both temperatures from both the cooling and the heating scans.

SCHEME 1

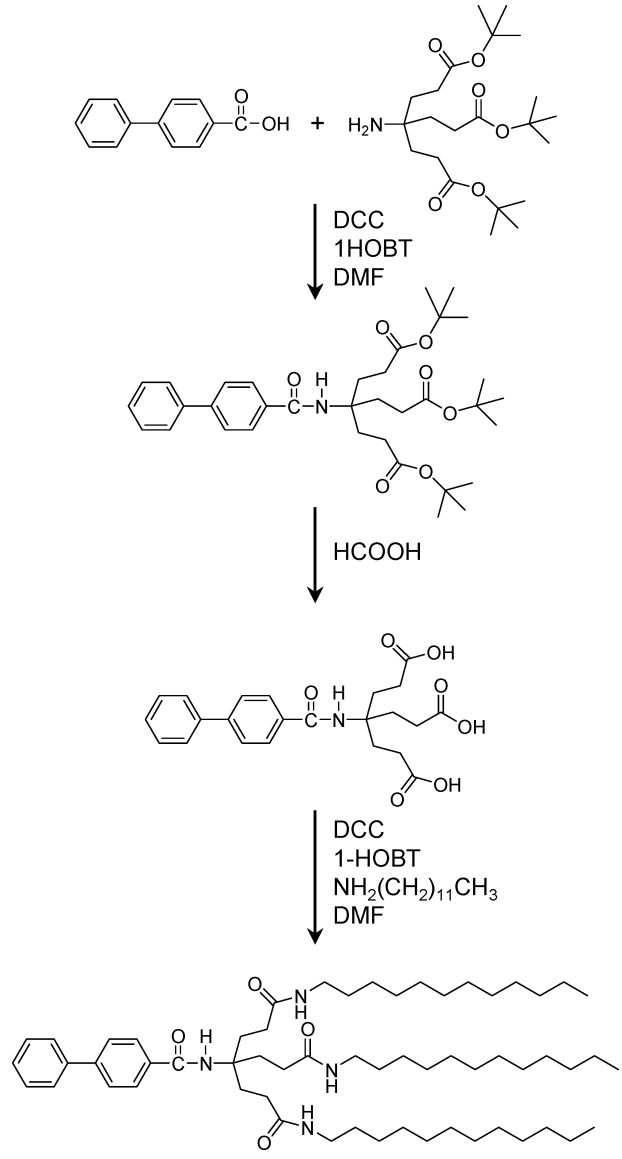

1D WAXD experiments were conducted in the reflection mode of a Rigaku 12 kW rotating-anode X-ray (Cu Kα radiation) generator coupled to a diffractometer. The diffraction peak positions and widths were calibrated with silicon crystals in the high 2θ-angle region (>15°) and silver behenate in the low 2θ-angle region. A hot stage was connected to the diffractometer in order to study the structural evolutions during heating and cooling. The temperature of hot stage was calibrated to be within ±1 °C. Samples were scanned across a 2θ-angle range of 1.5−35° at a scanning rate of 4°/min. The background scattering was subtracted from the sample scans.

Bright-field images of TEM (FEI Tacnai 12) were taken to examine crystal morphology on the nanometer length scale using an accelerating voltage of 120 kV. The camera length was set at 3 m and the SAED spacing smaller than 0.384 nm was calibrated using evaporated thallous chloride, which has a largest first-order spacing diffraction of 0.384 nm. The calibration of spacing values larger than 0.384 nm was conducted by doubling the *d* spacing of the first-order diffractions. Furthermore, the polyethylene (PE) surface lamellar decoration (SLD) technique was applied in order to study the surface topology of the self-assembled structure of asym-C_{12}PhA in the thin films. The PE decoration was conducted using linear PE as a decoration

material in a vacuum evaporator. The PE was degraded, evaporated, and deposited onto the surface of the self-assembled asym-C_{12}PhA columns.

Optical textures of the ordered phases were recorded at different temperatures with a POM (Olympus BH-2), which was coupled with a Mettler heating stage (FP-90). A tint retardation plate (530 nm) was placed between the objective lens and the eyepiece in order to identify the orientation of molecules in the POM textures. *H*-bonding and molecular chain conformations were analyzed using a FT IR (Digilab Win-IR Pro FTS 3000) containing a Bruker heating stage. The resolution was 1 cm^{-1}, and 40 scans were averaged for each spectrum. The temperatures of hot stage were calibrated to be within ±0.5 °C. The dynamics of each carbon and the conformations of the alkyl chains in asym-C_{12}PhA were also studied as a function of temperature using a solid-state ^{13}C NMR (Chemagnetics CMX 200) operated at 201.13 and 50.78 MHz for ^{1}H and ^{13}C nuclei. The samples were spun under nitrogen atmosphere at 4.5 kHz at the magic angle. The magic angle was optimized by the intensity calibration of the aromatic carbon resonance of hexamethylbenzene. The ^{13}C cross-polarization/magic angle spinning/dipolar decoupling (CP/MAS/DD) NMR spectra were acquired to selectively investigate the rigid components and the Bloch decay spectra with MAS/DD was used to study the mobile components.[23,25,44,46,51−55] The CP contact time was 1 ms, while the recycle time of the pulse was 5 s. Each spectrum consisted of an accumulation of 500 scans. The temperature of the solid-sate ^{13}C NMR experiment was controlled using a REX-F900 VT unit covering the range from −70 to 210 °C.

Overlapped C═O and N−H absorption peaks in FT IR, and characteristic carbon peaks in solid-state ^{13}C NMR were resolved using the PeakFit peak separation program (Jandel Scientific). Symmetric/asymmetric Gaussian and Lorentzian functions were used to obtain the best fit, respectively. The Cerius^2 (version 4.6) simulation software from Accelrys was used to calculate the minimal energy geometry of the asymmetrically tapered asym-C_{12}PhA compound in the isolated gas-phase utilizing the COMPASS force field.

Results and Discussion

Geometric Dimension and Shape of asym-C_{12}PhA. As shown in Figure 1a, the asymmetrically tapered asym-C_{12}PhA was programmed with three different parts: *H*-bonded hydrophilic amide moieties, a rigid hydrophobic biphenyl core, and three flexible hydrophobic alkyl chains. During self-assembly and self-organization processes, nanophase separation between rigid biphenyl rod and flexible alkyl tails might be enhanced because of *H*-bondable hydrophilic amide moieties. Furthermore, the asymmetric shape of asym-C_{12}PhA and relatively smaller volume of rigid biphenyl rod compared with hydrophobic alkyl chains can induce spatial steric hindrances, which might be one of the major factors to determine the molecular self-assembly of the asym-C_{12}PhA compound.

In order to estimate the spatial geometric figure and its dimensions of asymmetrically tapered asym-C_{12}PhA, the conformational energy minimization of asym-C_{12}PhA was conducted in the isolated vacuum state using Cerius^2 4.6 computer software. The global equilibrium geometry of asym-C_{12}PhA was constructed at 0 K using the COMPASS force field. The energy-minimized side (*yz* plane) and head (*xz* plane) views of asym-C_{12}PhA were illustrated in Figure 1b,c, respectively. Hydrophobic alkyl chains at one side of the rigid biphenyl rod were in the fully extended zigzag conformation at 145° with respect to the aromatic biphenyl rod. Consequently, asym-C_{12}PhA looks like a 3D cone with dimensions of 3.01 nm in height and 1.44 nm in bottom radius. This asymmetric 3D cone shape of asym-C_{12}PhA may induce a spatial steric hindrance during the molecular self-assembly process.

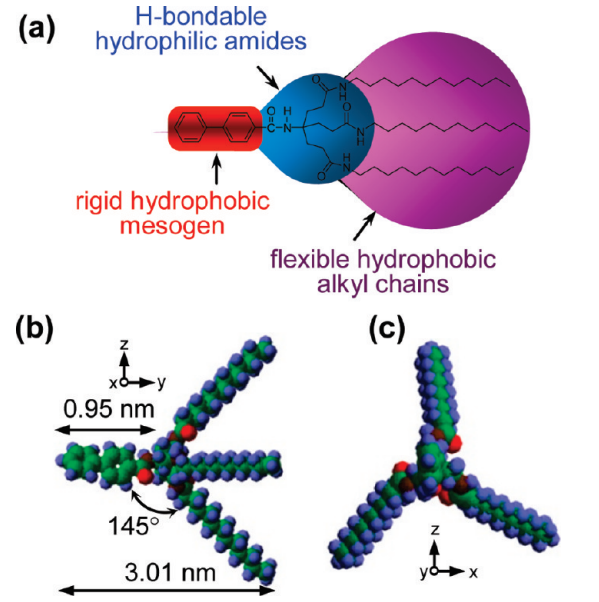

Figure 1. Schematic illustration of asym-C_{12}PhA compound (a). Computer energy-minimized dimensions and shapes of asym-C_{12}PhA with side (b) and head (c) views.

Thermal Properties of Phase Transformations of asym-C_{12}PhA. DSC experiments were first conducted during cooling and subsequent heating at scanning rates of 2.5−40 °C/min in order to detect various thermal transitions of asym-C_{12}PhA compound and to obtain quantitative thermodynamic properties of the thermal transitions. The results are shown in Figures 2a,b. During cooling at 2.5 °C/min, asym-C_{12}PhA exhibits two distinct exothermic peaks at 181 °C with −26 J/g (−24.2 kJ/mol) and 91 °C with −31 J/g (−28.8 kJ/mol), respectively. During the subsequent heating, a broad exothermic transition between 20 and 95 °C with −1 J/g (−0.9 kJ/mol) heat of transition and a sharp endothermic thermal transition at 188 °C with 58 J/g (53.9 kJ/mol) appeared. The endothermic transition during heating process could be attributable to the disorganization (melting) of the ordered structure developed during cooling and subsequent heating up to 95 °C. This statement can be supported by the simple calculation of the heats of transitions during the organization process (−24.2 kJ/mol + −28.8 kJ/mol + −0.9 kJ/mol = −53.9 kJ/mol) and during the melting process (53.9 kJ/mol), and by the observation of dark state at 190 °C under POM. The structural transition will be further confirmed by the WAXD experiments. It is noteworthy to point out that the exothermic peak at 181 °C during the cooling process was much less influenced than those of two subsequent exothermic thermal transitions at 91 °C during cooling and at ∼50 °C during subsequent heating, which is often observed during the transition from an isotropic phase to a highly ordered or a low ordered LC phase.[23−29,56−58]

Molecular Origins of the Phase Transformations of asym-C_{12}PhA. The possible molecular origins of structural evolutions were investigated using a combined FT IR and solid-state ^{13}C NMR experiments of asym-C_{12}PhA compound at different temperatures in the range of 30−230 °C. Figure 3a showed the FT IR spectrum of asym-C_{12}PhA at 30 °C. The N−H stretching vibration of amide groups exhibited a broad absorption band with the maximum intensity at 3293 cm^{-1}, and the amide I, II,

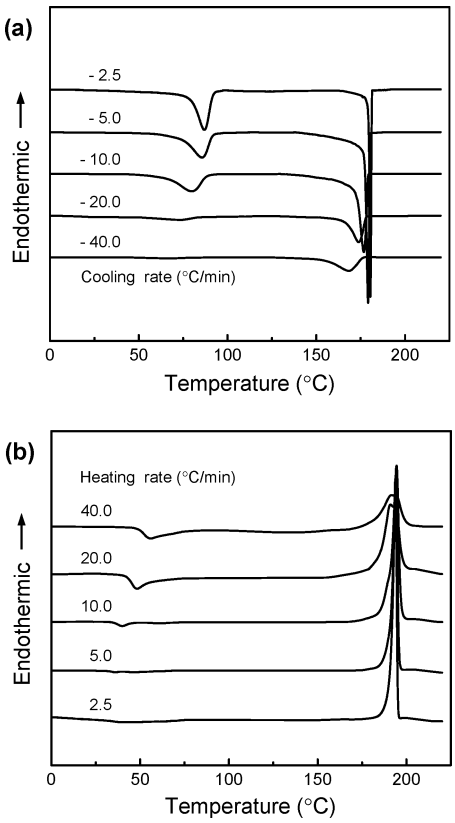

Figure 2. Sets of DSC cooling (a) and subsequent heating (b) thermal diagrams for asym-C_{12}PhA at scanning rates ranging from 2.5 to 40 °C/min.

and III motions generated absorption bands at 1638, 1548, and 1233 cm^{-1}, respectively.[44,45,59] The absorption bands for the alkyl chains were found at 2956 cm^{-1} for asymmetric stretching band of CH_3, 2924 cm^{-1} for asymmetric stretching band of CH_2, and 2873 cm^{-1} for symmetric stretching of CH_3, and 2853 cm^{-1} for symmetric stretching of CH_2.[44,45,59] Conformational change during phase transitions and molecular interactions of asym-C_{12}PhA was not examined because of low sensitivity. The *H*-bonding between the N−H group and the C═O group has been analyzed.[44,45,59] The N−H stretching vibration band at 3293 cm^{-1} and the carbonyl stretching vibration at 1638 cm^{-1} may build N−H···O═C *H*-bonds (Figure 3a). The intensity change of amide and carbonyl group was also studied during cooling and heating process at 2.5 °C/min. Two different spectral contribution bands were involved in the N−H stretching mode between 3200 and 3500 cm^{-1} (Figure 3b,c). The relatively weak and narrow band at 3448 cm^{-1} came from the free N−H groups, and the other broadband between 3200 and 3400 cm^{-1} was assigned to *H*-bonded N−H groups. The amide I mode is sensitive not only to *H*-bonds but also to local conformational changes.[59] The absorption peaks near 1600−1700 cm^{-1} were dominated by the carbonyl band, as illustrated in Figure 3b,c.[59] A narrow band between 1630 and 1650 cm^{-1} with a width at half-height of 24 cm^{-1} was originated from the *H*-bonded C═O groups in ordered domains, while a broadband between 1645 and 1670 cm^{-1} with a width at half-height of 45 cm^{-1} came from the *H*-bonded C═O groups in disordered domains. An absorption band between 1660 and 1690 cm^{-1} with a width at half-height of 35 cm^{-1} was due to the free C═O groups. During cooling, the absorption intensity of free N−H groups at 3448 cm^{-1} became weaker and concomitantly the area of *H*-bonded N−H groups increased with the gradual shift of maximum intensity from 3335 to 3293 cm^{-1}. Similarly, the intensity and area of free C═O band in the amide I mode was declined. According to Figure 3, more than 80% of amide groups formed the disordered *H*-bonds even in the isotropic phase. When the temperature was reduced to the high transition temperature at around 181 °C, the amount of free C═O groups and N−H groups was dropped below 10%, whereas the intensity and area of bands for *H*-bonded N−H and *H*-bonded C═O groups in ordered domains increased significantly. At 91 °C corresponding to low transition temperature, the intensity of *H*-bonded groups were further increased more than 95%. Upon subsequent heating up to 185 °C, the intensity of *H*-bonding in ordered domains gradually increased as shown in Figure 3c. This result was matched well with the exothermic thermal transitions in DSC thermogram (Figure 2b). When the temperature increased up to the endothermic thermal transition at 188 °C, the intensity of absorption bands for *H*-bonded N−H and C═O groups in ordered domains was abruptly dropped with the increases of the intensity of absorption bands of free N−H and C═O groups as well as of *H*-bonded C═O groups in disordered domains. Similar trends were continuously observed on further heating up to 230 °C, as shown in Figure 3b.

Asymmetric and symmetric stretching band of CH_2 at 2924 cm^{-1} and 2853 cm^{-1} can be attributed to the alkyl chain conformations of asym-C_{12}PhA. The peak changes were not so obvious to distinguish the trans−gauche transitions at different phases. Therefore, solid-sate ^{13}C NMR experiments with both CP/MAS/DD and Bloch decay methods were conducted to evaluate the ordered (all-trans) and disordered (mixture of trans and gauche) conformational changes of alkyl chains and the mobility of each carbon in asym-C_{12}PhA in different phases.[23,25,44,46,51−55] It is well-known that the CP/MAS/DD method is sensitive to the rigid components, whereas the mobile components can easily be detected by the Bloch decay method.[23,25,44,46,51−55] Chemical shift identifications by theoretical calculations based on the tabulated data accorded well with those of solid-state ^{13}C NMR experiments, as shown in Figure 4b.[59] The chemical shifts at 174 and 168 ppm resulted from the carbon atoms in the carbonyl groups attached at the end of biphenyl core and in the alkyl chains. The chemical shifts between 100 and 150 ppm came from the carbon atoms in the aromatic biphenyl groups. Additionally, the ^{13}C chemical shift at 57 ppm represented the carbon atoms at the α position, and the β and γ carbon atoms appeared at 32 and 24 ppm, respectively. The chemical shifts for other carbons were also identified as shown in Figure 4b. The β carbon chemical shift in the Bloch decay method (Figure 4c) consisted of two values resulting from all trans sequences (34−32 ppm) and gauche/trans random sequences (32−30 ppm) of the alkyl chains. The β chemical shift at 33 ppm corresponding to the methylene carbon atoms in the ordered segments of alkyl tails did not change much at 181 °C during cooling. When the temperature decreased below the low thermal transition temperature (91 °C), the amount of trans−trans conformation of β carbon suddenly increased from 25 to 75%. This result indicates that the methylene carbon atoms in the asym-C_{12}PhA are more or less in the disordered state before the low transition temperature, and therefore the exothermic transitions at 91 °C should be related with the organization of alkyl tails. These solid-sate ^{13}C NMR results further indicate that the exothermic peak at 181 °C during the cooling process is the transition from an isotropic phase to a highly ordered or a low ordered LC phase.

Identifications of Supra-Molecular Structures of asym-C_{12}PhA. The FT IR and solid-sate ^{13}C NMR results combined with DSC results provided molecular interactions in different

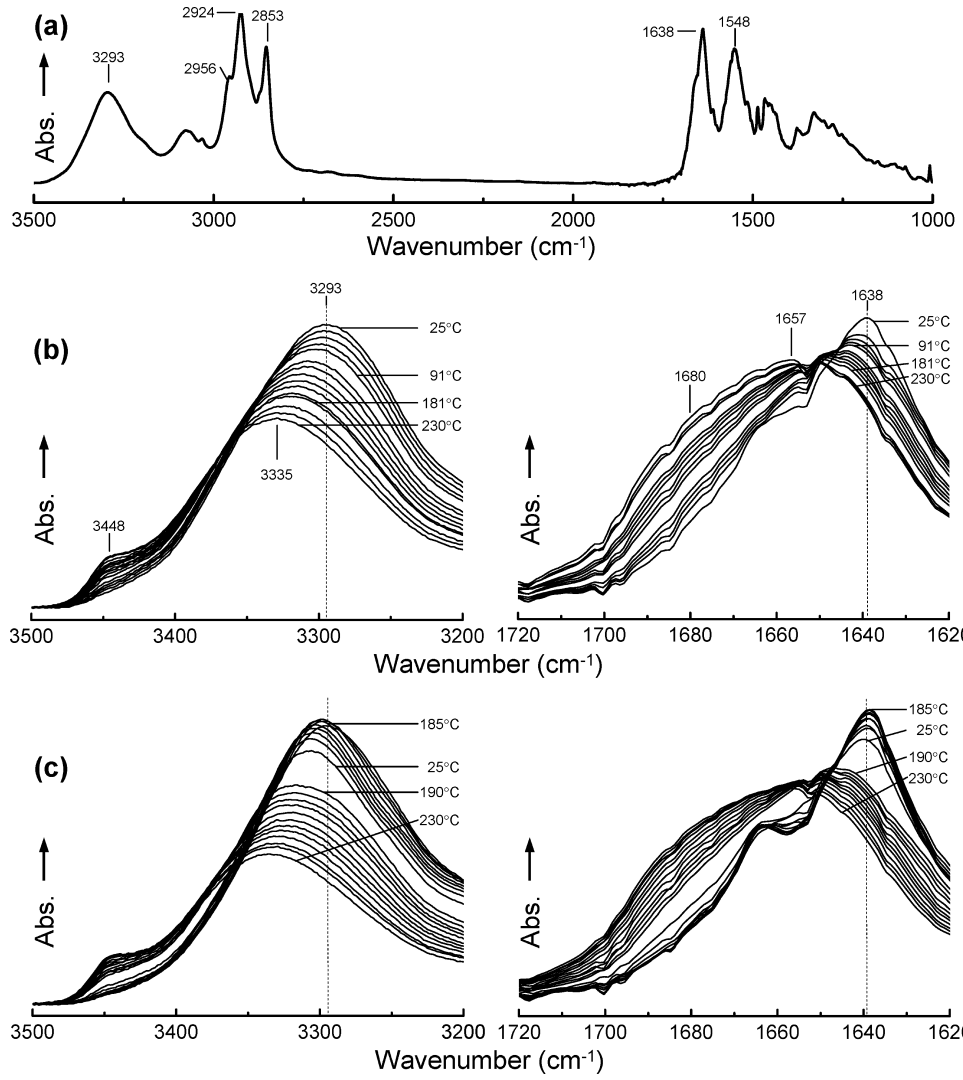

Figure 3. FT IR spectrum of asym-C_{12}PhA at room temperature after cooling from the isotropic phase at 2.5 °C/min (a). FT IR spectra of asym-C_{12}PhA during a cooling (b) and a subsequent heating (c) at the rate of 2.5 °C/min: 3500−3200 cm^{-1} (N−H) and 1720−1620 cm^{-1} (Amide I mode) regions between 230 and 25 °C.

phases of asym-C_{12}PhA on a molecular length scale. However these techniques did not provide direct information about structural changes. 1D WAXD experiments were carried out at different temperatures in order to monitor the corresponding structural evolutions of asym-C_{12}PhA. Figure 5a,b showed two sets of 1D WAXD powder patterns measured during cooling and subsequent heating process at a rate of 2.5 °C/min, respectively. Two different length scales, one is the nanometer scale in the low 2θ-angle region between 1.5° and 9° and the other on the subnanometer scale between 9° and 30°, can be identified. Above 181 °C, there were two amorphous halos, indicative of isotropic state. The peak in the low 2θ-angle region at $2\theta = 3.98°$ (d spacing = 2.22 nm) may correspond to the average periodicity of electron density fluctuations between the nanophase separated aromatic phenyl core and alkyl chains and the other in wide 2θ-angle region at $2\theta = 17.8°$ (d spacing = 0.498 nm) resulted from the average distance among the disordered alkyl chains. When the temperature reduced below 181 °C, three peaks at low angle start to appear at $2\theta = 3.10°$, 5.40°, and 6.20° (d spacing = 2.85, 1.64, and 1.43 nm, respectively) with two sharp reflections at $2\theta = 17.58°$ and 20.07° (d spacing = 0.505 and 0.442 nm, respectively) in the high 2θ-angle region. These WAXD results indicated that the phase below 181 °C is not a simple low-ordered LC phase but a highly ordered pseudo-3D LC phase. On the basis of the diffractions in this 1D WAXD pattern, the 2D a^*b^* lattice of the unit cell can be constructed to provide a highly ordered hexagonal columnar LC phase with unit cell dimensions of $a = b = 3.28$ nm, $c = 1.13$ nm, $\alpha = \beta = 90°$, and $\gamma = 60°$. It is worthy of reminding the fact that, on the basis of the solid-state ^{13}C NMR results of asym-C_{12}PhA, alkyl tails in asym-C_{12}PhA are more or less in a disordered state between 91 and 181 °C. As the temperature was reduced below the onset temperature of exothermic transition (91 °C), the intensities of reflections peaks were increased. The WAXD results are well-matched with the exothermic transition of DSC and the sudden increase of trans−trans conformations of alkyl tails detected by solid-state ^{13}C NMR during this exothermic thermal transition. During a subsequent heating process up to exothermic thermal transition at around 60 °C, the intensity of reflections in the high 2θ-angle region were continually increased, as shown in Figure 5b. Above 190 °C, all of the sharp reflections both in low and in high 2θ-angle regions disappeared, remaining two broad amorphous halos at $2\theta = 3.98°$ and 17.8°.

Even though the 1D WAXD powder experiments at different temperatures combined with the DSC, FT IR, and solid-state ^{13}C NMR results can monitor the structural evolutions in asym-C_{12}PhA, 1D WAXD results are limited to identify the 3D

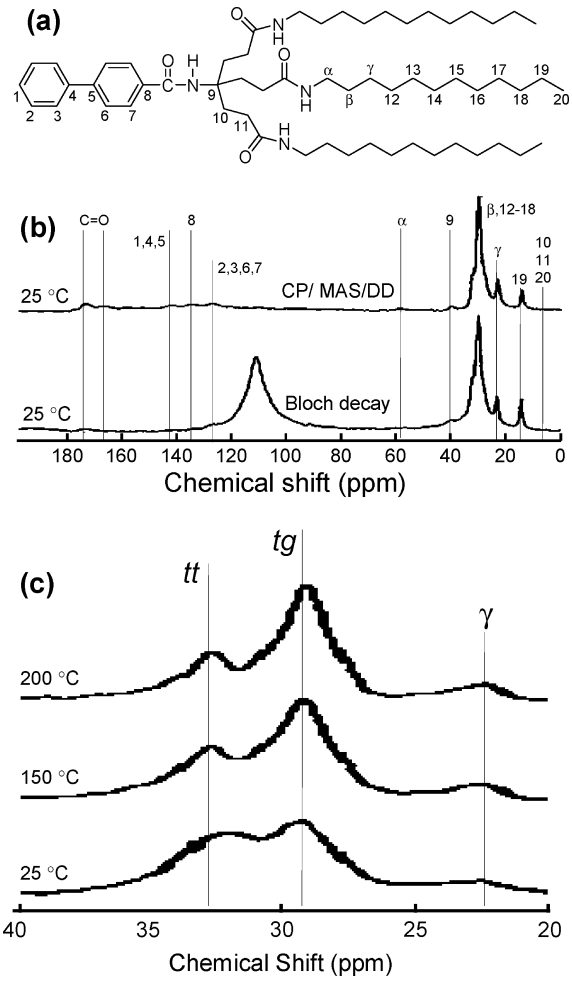

Figure 4. Sets of solid-state ^{13}C NMR spectra of asym-C_{12}PhA: CP/MAS/DD spectrum and Bloch decay spectrum between 0 and 200 ppm measured at 25 °C (b), and Bloch decay spectra at different temperatures between 20 and 40 ppm during cooling from 200 to 25 °C (c). Chemical shifts of each carbon in asym-C_{12}PhA were identified in a and b.

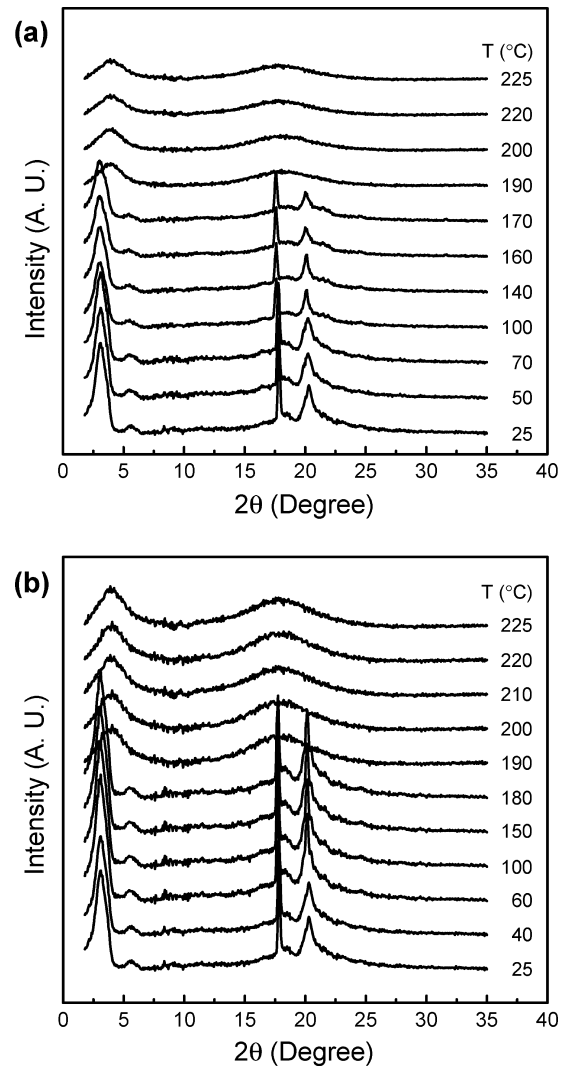

Figure 5. Sets of 1D WAXD powder patterns of asym-C_{12}PhA at a cooling (a) and a subsequent heating (b) at a rate of 2.5 °C/min at different temperatures.

ordered crystalline molecular structure. 1D WAXD should be supported by diffraction information from ordered domains. In order to identify the ordered molecular structure of asym-C_{12}PhA, thin film samples (50−150 nm) were prepared for TEM via solution casting from a 0.05% (w/v) chloroform solution onto carbon-coated mica. Figure 6a is a bright-field TEM image from a corner of an asym-C_{12}PhA spherulite, which is composed of thin ribbon-like single crystals. The long axis of a flat-on ribbon-like single crystal might be the growth direction because this is the radius direction of asym-C_{12}PhA spherulite. This speculation can be supported from SAED (Figure 6b). Without any sample tilting, the SAED image was taken from the circled area in Figure 6a. Combined with the results of 1D WAXD (Figure 5), c^* axis is assigned along the meridian direction, and the equator is parallel to the [$\bar{1}$10] direction. On the meridian, only one pair of weak diffraction is observed at d spacing = 0.376 nm, which can be the distance of the $\pi-\pi$ sacking interactions between aromatic biphenyl rings. This diffraction peak should be assigned as (003), and the (001) and (002) diffractions were extinct. This assignment can be supported by the series of diffractions in quadrant regions with indices of (hk1), (hk2), and (hk3). On the equator, there was one pair of strong diffractions at d spacing = 1.640 nm, which was identified to be ($\bar{3}$30). This assignment was also confirmed by the diffractions at (hk1), (hk2), and (hk3), and the high order diffractions of ($\bar{3}$30) located at d spacing = 0.820 nm and d spacing = 0.547 nm. Combined the ($\bar{3}$30) diffraction in SAED and the low 2θ-angle diffractions at $2\theta = 3.10°$ (d spacing = 2.85 nm) and $2\theta = 6.20°$ (d spacing = 1.43 nm) in WAXD, the 2D a^*b^* lattice of the unit cell can be constructed to provide a 3D crystalline unit cell with dimensions of $a = b = 9.84$ nm, $c = 1.13$ nm, $\alpha = \beta = 90°$, and $\gamma = 60°$ via the refinement of the reciprocal lattice,[60,61] and this phase was abbreviated as the Φ_{Cr} phase. Its calculated crystallographic density is 0.73 g/cm^3, which fits well with the measured one (0.72 g/cm^3).

On the basis of the WAXD and SAED results, the most possible molecular packing was proposed as shown in the schematic diagram of Figure 7a. A building block of the Φ_{Cr} phase can be constructed by three asym-C_{12}PhA compounds rotating 120° with respect to neighboring ones. However, in order to know the detail molecular packing and atom positions in the monoclinic unit cell, computer simulation in both real and reciprocal spaces should be carried out,[24,26,43,56] which is under investigation. Three major driving forces in the formation of a building block of the Φ_{Cr} phase were the H-bonds between N—H and C═O groups, the nanophase separation between the aromatic biphenyl rods and the alkyl chains, and the $\pi-\pi$ stacking interactions between aromatic biphenyl rods. The hydrophilic amide moieties between a rigid hydrophobic biphenyl rod and flexible hydrophobic alkyl chains will enhance

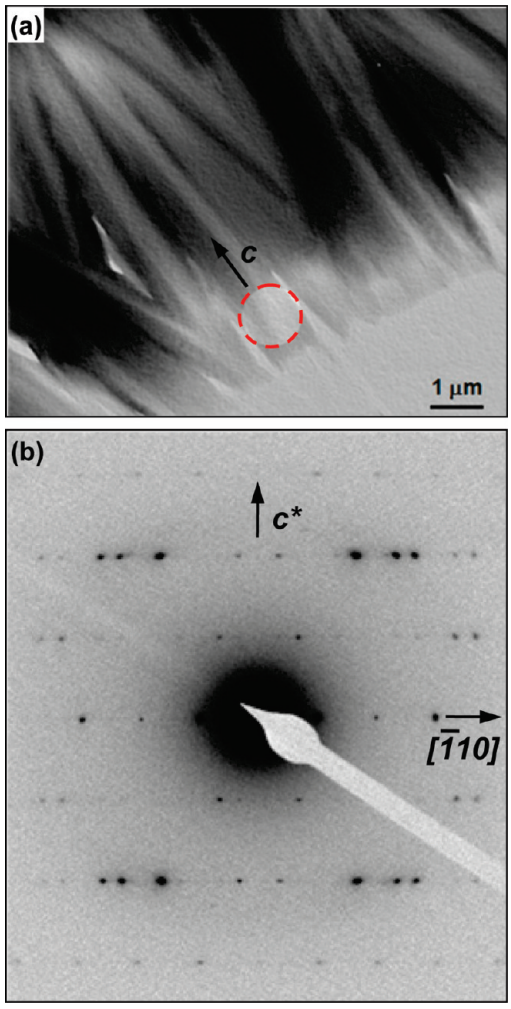

Figure 6. Bright-field TEM image of the highly ordered columnar crystalline phase (Φ_{Cr}) of asym-C_{12}PhA (a). (a) The arrow is pointing along the long axis of the columns (*c* axis). SAED pattern (b) from the circled area of the bright-field TEM morphology in a.

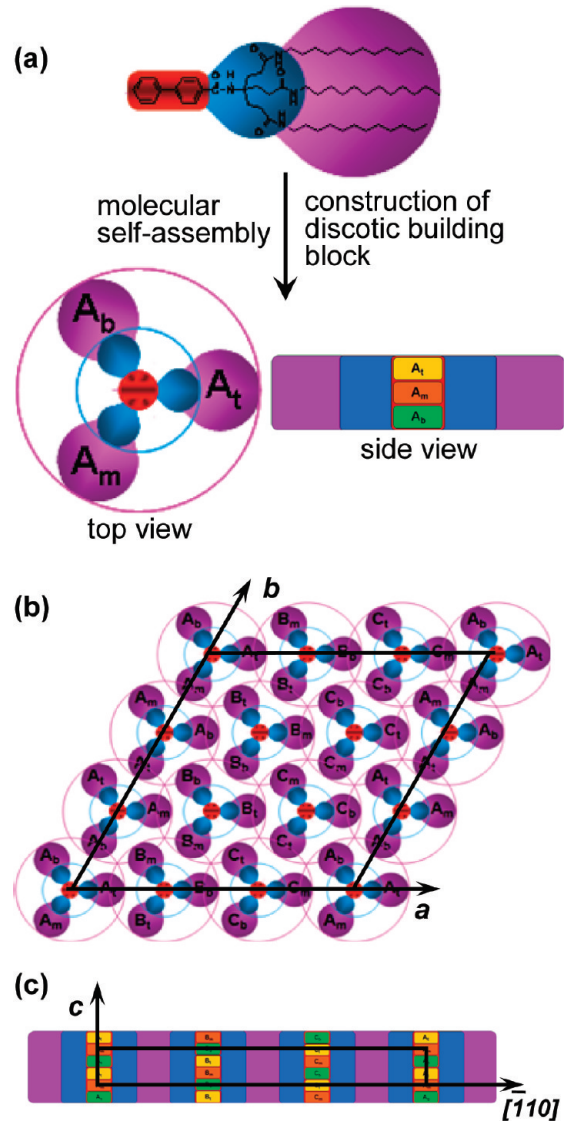

Figure 7. Schematic illustrations of the discotic building blocks by the molecular self-assembly process (a) and the columnar crystalline phase (Φ_{Cr}) of asym-C_{12}PhA by self-organization process in [001] zone (b) and [1̄10] zone (c).

the nanophase separation. In addition to $\pi-\pi$ stacking interactions between biphenyl rings, the intra/intermolecular *H*-bonds stabilizes the ordered structure. During the molecular self-assembly process for a supra-molecular discotic building block, a spatial steric hindrance originated from the relatively big alkyl chains in volume compared with the aromatic biphenyl rod should be accounted for. Therefore, the discotic building blocks of the Φ_{Cr} phase was constructed by molecular self-assembly process, where the tmb (top-middle-bottom) stacked discotic building block further self-assembled into columns, and these columns were laterally self-organized to provide Φ_{Cr} crystalline phase. Molecular arrangement in the Φ_{Cr} crystalline was schematically illustrated in Figure 7b (top-view, [001] zone),c (side-view, [1̄1̄0] zone), which showed the good agreement with the diffraction results of WAXD (Figure 5) and SAED (Figure 6b).

In order to further support the asym-C_{12}PhA packing model in the [1̄1̄0] zone (Figure 7c), the PE lamellar surface decoration experiment was conducted on the surface of the Φ_{Cr} single crystals.[62,63] The result was shown in Figure 8. In this figure, the PE crystalline rods were perpendicular to *c* axis which was parallel to the long axis of columns. This indicates that the chain axes of the PE oligomers are recognized as the columnar axis and thus deposited along the *c* axis. This surface topological information of the Φ_{Cr} crystalline phase agreed well with the proposed molecular packing model (Figure 7c) which was similar to the results reported previously.[29,43]

The macroscopic molecular orientation of the Φ_{Cr} crystalline phase was observed utilizing POM. Figure 9a showed the POM micrograph of asym-C_{12}PhA prepared by mechanical shearing just below the onset temperature of the high thermal transition (181 °C) and further cooling to 25 °C. The oriented asym-C_{12}PhA film was heated up to 90 °C in order to maximize the organization. As shown in Figure 9a, cracks in micrometer length scale were generated perpendicular to the shear direction (SD), suggestive of the volume shrinkage along the *c* axis during the crystallization process of alkyl tails.[29,43,64] A tint retardation plate (530 nm) was also applied between objective lenses and eyepieces in order to identify the orientation of molecules in the POM textures, as shown in Figure 9b. The sheared film was turn to yellow, which means that the refractive index perpendicular to the SD ($n_\perp$) is higher than parallel one ($n_\parallel$).[29,43] Therefore, the column direction of this supra-molecular columnar phase should align along the shear direction. This observation is also consistent with the results of SAED (Figure 6b) and bight-field TEM image of PE decorated Φ_{Cr} crystals (Figure 8).

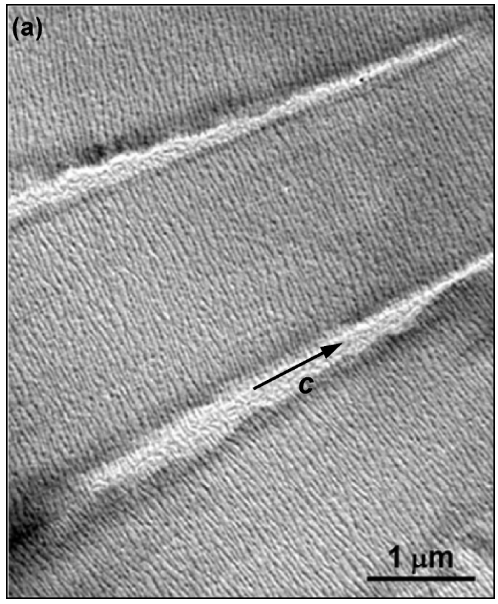

Figure 8. Bright-field TEM morphology after the PE surface lamellar decoration on the Φ_{Cr} crystals. The arrow points along the long axis of the columns (*c* and *c** axis).

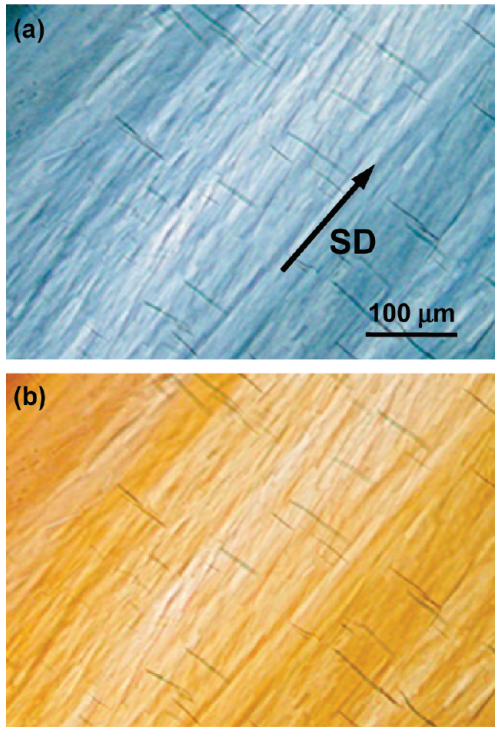

Figure 9. POM morphological observations of Φ_{Cr} crystals (a) and POM texture with a tint plate between an objective lens and an eyepiece (b). The arrow points along the shear direction (SD, *c* axis).

When a thin film of asym-C_{12}PhA compound was increased above the isotropic temperature (181 °C) and cooled down to room temperature at a relatively fast cooling rate (above 20 °C/min), asym-C_{12}PhA fibers with ~1 μm in diameter and several millimeters in length were formed (Figure 10a). The fiber was not a single crystal but was made of several tiny crystals, which was obvious in the magnified bight-field TEM image (Figure 10b). In order to study molecular orientation in these fibers, the PE lamellar decoration technique was applied once again. The bight-field TEM image of asym-C_{12}PhA fibers (Figure 11a) and its expended TEM image (Figure 11b) clearly indicated

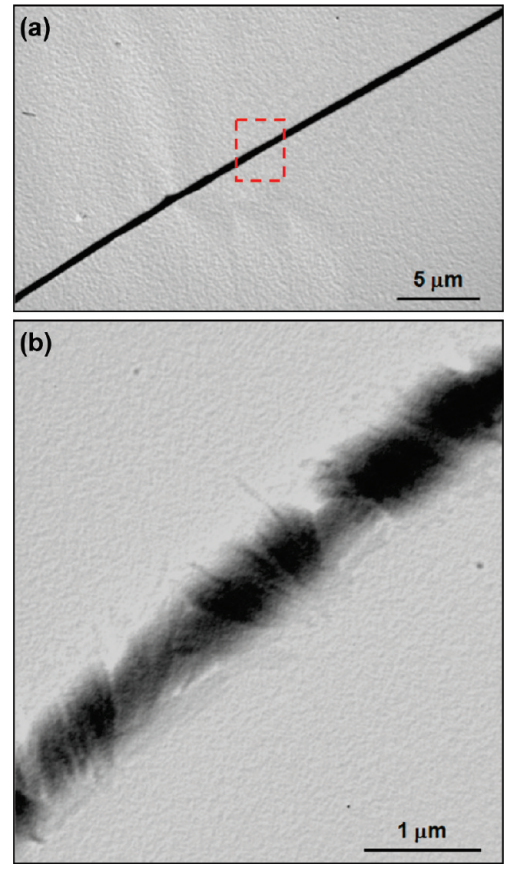

Figure 10. Bright-field TEM image of the Φ_{Cr} which was prepared by cooling the isotropic state of asym-C_{12}PhA to room temperature at a relatively fast cooling rate (20 °C/min) (a). (b) The magnified bright-field TEM image of a.

that the self-assembled asym-C_{12}PhA fibers were braids of tiny single crystals. The origin of fiber formation by gathering small single crystals could be related with the diffusion of molecules during the self-organization processes,[65] which is under investigation.

Conclusions

Phase behaviors and the corresponding structures of a synthesized asymmetrically tapered *N,N′-tris*[[(2-dodecylaminocarbonyl)ethyl]methyl]-4-biphenylamide (as asym-C_{12}PhA) have been investigated on the basis of various experimental techniques. From the combined SAED, DSC, FT IR, and sold-state ^{13}C NMR results, we identified that the discotic building block was constructed by three asym-C_{12}PhA biphenylamides rotating 120° with respect to neighboring ones and the tmb stacked discotic building blocks further self-assembled into columns, and then these assembled columns were laterally close-packed to provide a highly ordered hexagonal columnar mesophase by a self-organization process. After the low transition temperature, alkyl tails around the columns were crystallized and gave the 3D columnar crystalline phase (Φ_{Cr}). Three major driving forces for the formation of the Φ_{Cr} phase includes the *H*-bonds between N−H and C═O groups, the nanophase separation between the aromatic biphenyl rods and the alkyl tails, and the $\pi-\pi$ stacking interactions between aromatic biphenyl rods. Phase identifications were further supported by the texture changes in POM, and molecular arrangements were also investigated by introducing a tint plate. By utilizing

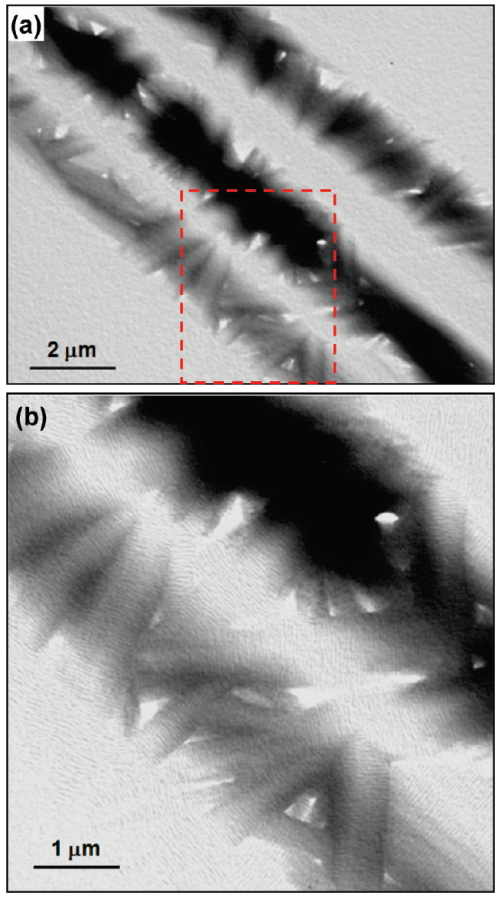

Figure 11. Bright-field TEM image after the PE surface lamellar decoration on the asym-C_{12}PhA Φ_{Cr} crystal fibers (a). (b) The magnified bright-field TEM image of a.

polyethylene surface decoration technology, it was identified that the self-assembled asym-C_{12}PhA fibers were constructed by the aggregation of tiny single crystals.

Acknowledgment. This research was supported by National Space Laboratory program (KSEF-S108A01003210, Korea) and Basic Science Research program (NRF-2009-0065121, Korea) funded by the Korean government (MEST).

References and Notes

(1) Sage, I. C. *Handbook of Liquid Crystals*; Demus, D., Goodby, J., Gray, G. W., Spiess, H.-W., Vill, V., Eds.; Wiley-VCH: Weinheim, 1998; Vol. 1, pp. 731−762.
(2) Cammidge, A. N.; Bushby, R. J. *Handbook of Liquid Crystals*; Demus, D., Goodby, J., Gray, G. W., Spiess, H.-W., Vill, V., Eds.; Wiley-VCH: Weinheim, 1998; Vol. 2B, pp. 693−748.
(3) Chandrasekhar, S. *Handbook of Liquid Crystals*; Demus, D., Goodby, J., Gray, G. W., Spiess, H.-W., Vill, V., Eds.; Wiley-VCH: Weinheim, 1998; Vol. 2B, pp. 749−780.
(4) Tang, B. Y.; Jing, A. J.; Li, C. Y.; Shen, Z.; Wang, H.; Harris, F. W.; Cheng, S. Z. D. *Cryst. Growth Des.* **2003**, *3*, 375.
(5) Boden, N.; Bushby, R. J.; Clements, J. *J. Chem. Phys.* **1993**, *98*, 5920.
(6) Arikainen, E. O.; Boden, N.; Bushby, R. J.; Clements, J.; Movaghar, B.; Wood, A. *J. Mater. Chem.* **1995**, *5*, 2161.
(7) Matsui, T.; Nagata, T.; Ozaki, M.; Fujii, A.; Onoda, M.; Teraguchi, M.; Masuda, T.; Yoshino, K. *Synth. Met.* **2001**, *119*, 599.
(8) Adam, D.; Closs, F.; Frey, T.; Funhoff, D.; Haarer, D.; Ringsdorf, H.; Schuhmacher, P.; Siemensmeyer, K. *Phys. Rev. Lett.* **1993**, *70*, 457.
(9) Adam, D.; Schuhmacher, P.; Simmerer, J.; Haussling, L.; Siemensmeyer, K.; Etzbach, K. H.; Ringsdorf, H.; Haarer, D. *Nature* **1994**, *371*, 141.
(10) Bengs, H.; Closs, F.; Frey, T.; Funhoff, D.; Ringsdorf, H.; Siemensmeyer, K. *Liquid Cryst.* **1993**, *15*, 565.
(11) Closs, F.; Siemensmeyer, K.; Frey, T.; Funho, D. *Liquid Cryst.* **1993**, *14*, 629.
(12) Boden, N.; Bushby, R. J.; Clements, J.; Movaghar, B.; Donovan, K. J.; Kreouzis, T. *Phys. Rev. B* **1995**, *52*, 13274.
(13) Simmerer, J.; Glusen, B.; Paulus, W.; Kettner, A.; Schuhmacher, P.; Adam, D.; Etzbach, K.; Siemensmeyer, K.; Wendorff, J. H.; Ringsdorf, H.; Haarer, D. *Adv. Mater.* **1996**, *8*, 815.
(14) Bock, H.; Helfrich, W. *Liquid Cryst.* **1992**, *12*, 697.
(15) Bock, H.; Helfrich, W. *Liquid Cryst.* **1995**, *18*, 387.
(16) Tschierske, C. *J. Mater. Chem.* **1998**, *8*, 1485.
(17) Ichimura, K. *Chem. Rev.* **2000**, *100*, 1847.
(18) Sokolov, A. N.; Friscic, T.; Blais, S.; Ripmeester, J. A.; MacGillivray, N. R. *Cryst. Growth Des.* **2006**, *6*, 2427.
(19) Johansson, R.; Ohrstrom, L.; Wendt, O. F. *Cryst. Growth Des.* **2007**, *7*, 1974.
(20) Saez, I. M.; Goodby, J. W. *J. Mater. Chem.* **2005**, *15*, 26.
(21) Zhu, Y.-Y.; Wu, J.; Li, C.; Zhu, J.; Hou, J.-L.; Li, C.-Z.; Jiang, X.-K.; Li, Z.-T. *Cryst. Growth Des.* **2007**, *7*, 1490.
(22) Cannon, A. S.; Warner, J. C. *Cryst. Growth Des.* **2002**, *2*, 255.
(23) Jeong, K.-U.; Jin, S.; Ge, J. J.; Knapp, B. S.; Graham, M. J.; Ruan, J.; Guo, M.; Xing, H.; Harris, F. W.; Cheng, S. Z. D. *Chem. Mater.* **2005**, *17*, 2852.
(24) Jeong, K.-U.; Knapp, B. S.; Ge, J. J.; Jin, S.; Graham, M. J.; Xiong, H.; Harris, F. W.; Cheng, S. Z. D. *Macromolecules* **2005**, *38*, 8333.
(25) Jeong, K.-U.; Knapp, B. S.; Ge, J. J.; Jin, S.; Graham, M. J.; Harris, F. W.; Cheng, S. Z. D. *Chem. Mater.* **2006**, *18*, 680.
(26) Jeong, K.-U.; Knapp, B. S.; Ge, J. J.; Graham, M. J.; Tu, Y.; Leng, S.; Xiong, H.; Harris, F. W.; Cheng, S. Z. D. *Polymer* **2006**, *47*, 3351.
(27) Jeong, K.-U.; Yang, D. K.; Graham, M. J.; Tu, Y.; Kuo, S. W.; Knapp, B. S.; Harris, F. W.; Cheng, S. Z. D. *Adv. Mater.* **2006**, *18*, 3229.
(28) Jeong, K.-U.; Jing, A. J.; Monsdorf, B.; Graham, M. J.; Harris, F. W.; Cheng, S. Z. D. *Chem. Mater.* **2007**, *19*, 2921.
(29) Jeong, K.-U.; Jing, A. J.; Monsdorf, B.; Graham, M. J.; Harris, F. W.; Cheng, S. Z. D. *J. Phys. Chem. B* **2007**, *110*, 767.
(30) Jeong, S. J.; Sureshkumar, P.; Jeong, K.-U.; Lee, S. H.; Jeong, S. H.; Lee, Y. E.; Lu, R.; Wu, S. T. *Optics Express* **2007**, *15*, 11698.
(31) Wang, L.; Jeong, K.-U.; Lee, M.-H. *J. Mater. Chem.* **2008**, *18*, 2657.
(32) Yang, D.-K.; Jeong, K.-U.; Cheng, S. Z. D. *J. Phys. Chem. B* **2008**, *112*, 1358.
(33) Hunter, C. A.; Sanders, J. K. M. *J. Am. Chem. Soc.* **1990**, *112*, 5525.
(34) Lehn, J. M. *Science* **2002**, *295*, 2400.
(35) Messmore, B. W.; Sukerkar, P. A.; Stupp, S. I. *J. Am. Chem. Soc.* **2005**, *127*, 7992.
(36) MacDonald, J. C.; Pieter, C.; Dorrestein, P. C.; Malissa, M.; Pilley, M. M. *Cryst. Growth Des.* **2001**, *1*, 29.
(37) Hirschberg, J. H.; Brunsveld, L.; Ramzi, A.; Vekemans, J. A.; Sijbesma, R. P.; Meijer, E. W. *Nature* **2000**, *407*, 167.
(38) Kato, T.; Mizoshita, N.; Kanie, K. *Macromol. Rapid Commun.* **2001**, *22*, 797.
(39) Kato, T. *Science* **2002**, *295*, 2414.
(40) Reinhoudt, D. N.; Drego-Calama, M. *Science* **2002**, *295*, 2403.
(41) Brewer, J. T.; Parkin, S.; Grossman, R. B. *Cryst. Growth Des.* **2004**, *4*, 591.
(42) Ungar, G.; Abramic, D.; Percec, V.; Heck, J. A. *Liquid Cryst.* **1996**, *21*, 73.
(43) Xue, C.; Jin, S.; Weng, X.; Ge, J. J.; Shen, Z.; Shen, H.; Graham, M. J.; Jeong, K.-U.; Huang, H.; Zhang, D.; Guo, M.; Harris, F. W.; Cheng, S. Z. D. *Chem. Mater.* **2004**, *16*, 1014.
(44) Shen, H.; Jeong, K.-U.; Xiong, H.; Graham, M. J.; Leng, S.; Zheng, J. X.; Huang, H.; Guo, M.; Harris, F. W.; Cheng, S. Z. D. *Soft Matter* **2006**, *2*, 232.
(45) Shen, H.; Jeong, K.-U.; Graham, M. J.; Leng, S.; Huang, H.; Lotz, B.; Hou, H.; Harris, F. W.; Cheng, S. Z. D. *J. Macrom. Sci., Part B: Phys.* **2006**, *45*, 215.
(46) Hwang, S.-H.; Park, S.-J.; Kim, H.-Y.; Kuo, S.-W.; Lee, S.-H.; Lee, M.-H.; Jeong, K.-U. *J. Phys. Chem. B* **2009**, *113*, 5843.
(47) Klausner, Y. S.; Bodansky, M. *Synthesis* **1972**, 453.
(48) Newkome, G. R.; Moorefield, C. N.; Baker, G. R. *Aldrichimica Acta* **1992**, *25*, 31.
(49) Newkome, G. R.; Weis, C. D. *Org. Prep. Proc. Int.* **1996**, *28*, 242.
(50) Han, S.-Y.; Kim, Y.-A. *Tetrahedron* **2004**, *60*, 2447.
(51) Bovey, F. A.; Mirau, P. A. *NMR of Polymers*, Academic Press: San Diego, 1996.
(52) Cheng, J.; Jin, Y.; Wunderlich, B.; Cheng, S. Z. D.; Yandrasits, M. A.; Zhang, A.; Percec, V. *Macromolecules* **1992**, *25*, 5991.
(53) Cheng, J.; Yoon, Y.; Ho, R.-M.; Leland, M.; Guo, M.; Cheng, S. Z. D.; Chu, P.; Percec, V. *Macromolecules* **1997**, *30*, 4688.
(54) McElheny, D.; Grinshtein, J.; Frydman, V.; Frydman, L. *Macromolecules* **2002**, *35*, 3544.

(55) Ishida, H.; Horii, F. *Macromolecules* **2002**, *35*, 5550.
(56) Ye, C.; Xu, G.; Yu, Z. Q.; Lam, J. W. Y.; Jang, J. H.; Peng, H. L.; Tu, Y.; Liu, Z. F.; Jeong, K.-U.; Cheng, S. Z. D.; Chen, E.-Q.; Tang, B. Z. *J. Am. Chem. Soc.* **2005**, *127*, 7668.
(57) Ruan, J.-J.; Ge, J. J.; Jin, S.; Jeong, K.-U.; Graham, M. J.; Zhang, D.; Harris, F. W.; Lotz, B.; Cheng, S. Z. D.*Polymer* **2006**, *47*, 4182.
(58) Jin, S.; Jeong, K.-U.; Li, C. Y.; Bai, F.; Harris, F. W.; Cheng, S. Z. D.; Lotz, B. *Macromolecules* **2007**, *40*, 5450.
(59) Pavia, D. L.; Lampman, G. M.; Kriz, G. S. *Introduction to Spectroscopy*, 2nd Eds.; Harcourt Brace College Publishers: Austin, 1996.
(60) Eashoo, M.; Wu, Z.; Zhang, A.; Shen, D.; Tse, C.; Harris, F. W.; Cheng, S. Z. D.; Gardner, K. H.; Hsiao, B. S. *Macromol. Chem. Phys.* **1994**, *195*, 2207.
(61) Leng, S.; Wex, B.; Chan, L. H.; Graham, M. J.; Jin, S.; Jing, A. J.; Jeong, K.-U.; Van Horn, R. M.; Sun, B.; Zhu, M.; Kaafarani, B. R.; Cheng, S. Z. D. *J. Phys. Chem. B* **2009**, *113*, 5403.
(62) Wittmann, J.-C.; Lotz, B. *Makromol. Chim. Rapid Commun.* **1982**, *3*, 733.
(63) Wittmann, J.-C.; Lotz, B. *J. Polym. Sci. Polym. Phys. Ed.* **1985**, *23*, 205.
(64) Dierking, I. *Textures of Liquid Crystals*, Wiley-VCH: Weinheim, 2003.
(65) Cheng, S. Z. D. *Phase Transitions in Polymers: The Role of Metastable States*, Elsevier: Amsterdam, 2008.

JP905672S